Thermal Rate Constant for H + CH_3 → CH_4 Recombination. 3. Comparison of Experiment and Canonical Variational Transition State Theory

William L. Hase,*† Sandra L. Mondro,† Ronald J. Duchovic,‡ and David M. Hirst§

Contribution from the Department of Chemistry, Wayne State University, Detroit, Michigan 48202, Theoretical Chemistry Group, Chemistry Division, Argonne National Laboratory, Argonne, Illinois 60439, and Department of Chemistry, University of Warwick, Coventry CV4 7AL, United Kingdom. *Received November 5, 1986*

Abstract: Canonical variational transition state theory is used to calculate bimolecular rate constants for H + CH_3 and D + CH_3 recombination. The calculations are performed on an analytic potential energy surface derived from recent ab initio calculations. Rate constants calculated for this surface are in very good agreement with the experimental values. The H(D)---CH_3 transitional rocking modes are treated as quantum harmonic oscillators or classical hindered rotors in the calculations. These two treatments give rate constants which agree to within 15%. The variational transition states become tighter as the temperature is increased.

I. Introduction

It is well-known that the variational form of transition state theory is needed to model neutral–neutral association reactions.[1-6] The general application of this theoretical approach has in part been limited by the availability of accurate potential energy surfaces. Two potential energy surface properties which are particularly important are the minimum energy path potential and the neutral–neutral anisotropic angular/bending potential. This latter property gives rise to transitional rocking modes which transform from free rotations to vibrations as the neutral reactants associate.[2,3,7,8] To apply variational transition state theory, energy levels, densities of state, and partition functions are required for these modes as functions of the reaction coordinate.[1-9]

The above potential energy surface properties are difficult to calculate accurately by ab initio methods, and one approach has been to model them by semiempirical functions.[2,3,8] For example, the minimum energy path potential has been represented by a Morse oscillator, and bond-energy–bond-order (BEBO) type functions have been used to model the change in the vibrational/rotational frequencies for the transitional rocking modes vs. reaction coordinate. Though recent ab initio calculations indicate that these semiempirical functions may not represent the actual shape of neutral–neutral potential energy surfaces,[10-15] they are still sufficiently flexible to fit association rate constants.[8]

The H + CH_3 → CH_4 reaction is particularly important since it is the simplest alkyl radical/atom association reaction. An analytic potential energy function has been derived for this reaction and fit to MP4/6-31G** ab initio calculations.[11] This surface has been used in classical trajectory[16a] and variational transition state theory calculations of the H + CH_3 → CH_4 rate constant[16b] and in a Monte Carlo transition-state study of CH_4 dissociation.[17]

In the MP4 ab initio calculations it was found that the CH bond stretching potential rises more steeply than that given by the Morse function.[11] The ab initio potential may be fitted by a generalized Morse function,[10,18] in which the exponential parameter β is fit by a cubic polynomial. More recent ab initio calculations, at higher levels of theory,[12-15] show that the MP4 calculations over-accentuate the steepness of the CH stretching potential. However, these calculations still show that the potential is significantly steeper than the Morse function.

In the work presented here, the H + CH_3 ⇄ CH_4 analytic potential energy surface derived by Duchovic et al.[11] is modified to fit the recent MRD–CI (multireference double excitation) calculations of Hirst[13] in which the 6-31G** basis is used. The H + CH_3 → CH_4 and D + CH_3 → CH_3D bimolecular rate constants are determined for this surface with canonical variational transition state theory for temperatures in the 200–1000 K range and compared with experimental measurements.[19] To evaluate the sensitivity of the canonical variational transition state theory rate constant to potential energy surface details, calculations are also presented for surfaces which fit the CH stretching potentials calculated by Brown and Truhlar[12] at the MRD–CI level with diffuse and bond polarization functions supplementing the 6-31G** basis and by Schlegel[14] in which spin contamination is removed from the MP4/6-31G** wave function.

II. Potential Energy Surface

The analytic potential energy function used here for the calculation of the H + CH_3 → CH_4 biomolecular rate constant is that derived by Duchovic et al.[11b] A number of parameters in this surface are changed to fit recent accurate ab initio calculations

† Wayne State University.
‡ Argonne National Laboratory.
§ University of Warwick.

(1) Bunker, D. L.; Pattengill, M. *J. Chem. Phys.* **1968**, *48*, 772.
(2) (a) Hase, W. L. *J. Chem. Phys.* **1972**, *57*, 730. (b) Hase, W. L. *J. Chem. Phys.* **1976**, *64*, 2442.
(3) (a) Gaedtke, H.; Troe, J. *Ber Bunsenges. Phys. Chem.* **1973**, *77*, 24. (b) Quack, M.; Troe, J. *Ber. Bunsenges. Phys. Chem.* **1974**, *78*, 240. (c) Quack, M.; Troe, J. *Ber. Bunsenges. Phys. Chem.* **1977**, *81*, 329.
(4) Truhlar, D. G.; Garrett, B. C. *Acc. Chem. Res.* **1980**, *13*, 440.
(5) Hase, W. L. *Acc. Chem. Res.* **1983**, *16*, 258.
(6) Rai, S. N.; Truhlar, D. G. *J. Chem. Phys.* **1983**, *79*, 6046.
(7) Wardlaw, D. M.; Marcus, R. A. *Chem. Phys. Lett.* **1984**, *110*, 230. Wardlaw, D. M.; Marcus, R. A. *J. Chem. Phys.* **1985**, *83*, 3462.
(8) (a) Cobos, C. J.; Troe, J. *Chem. Phys. Lett.* **1985**, *113*, 419. (b) Cobos, C. J.; Troe, J. *J. Chem. Phys.* **1985**, *83*, 1010. (c) Troe, J. *J. Phys. Chem.* **1986**, *90*, 3485. (d) Troe, J., private communication.
(9) Pacey, P. D. *J. Chem. Phys.* **1982**, *77*, 3540. LeBlanc, J. F.; Pacey, P. D. *J. Chem. Phys.* **1985**, *83*, 4511.
(10) Wright, J. S.; Shih, S.-K. *J. Chem. Phys.* **1980**, *73*, 5204. Wright, J. S.; Donaldson, D. J.; Williams, R. J. *J. Chem. Phys.* **1984**, *81*, 397. Wright, J. S.; Donaldson, D. J. *Chem. Phys.* **1985**, *94*, 15.
(11) (a) Duchovic, R. J.; Hase, W. L.; Schlegel, H. B.; Frisch, M. J.; Raghavachari, K. *Chem. Phys. Lett.* **1982**, *89*, 120. (b) Duchovic, R. J.; Hase, W. L.; Schlegel, H. B. *J. Phys. Chem.* **1984**, *88*, 1339. (c) Duchovic, R. J.; Hase, W. L. *Chem. Phys. Lett.* **1984**, *110*, 474.
(12) Brown, F. B.; Truhlar, D.G. *Chem. Phys. Lett.* **1985**, *113*, 441.
(13) Hirst, D. M. *Chem. Phys. Lett.* **1985**, *122*, 225.
(14) Schlegel, H. B. *J. Chem. Phys.* **1986**, *84*, 4530.
(15) Peyerimhoff, S.; Lewerenz, M.; Quack, M. *Chem. Phys. Lett.* **1984**, *109*, 563. Evleth, E. M.; Kassab, E. *Chem. Phys. Lett.* **1986**, *131*, 475.
(16) (a) Part I in this series: Duchovic, R. J.; Hase, W. L. *J. Chem. Phys.* **1985**, *82*, 3599. (b) Part II in this series: Hase, W. L.; Duchovic, R. J. *J. Chem. Phys.* **1985**, *83*, 3448.
(17) Viswanathan, R.; Raff, L. M.; Thompson, D. L. *J. Chem. Phys.* **1985**, *82*, 3083.
(18) Whitton, W. N.; Kuntz, P. J. *J. Chem. Phys.* **1976**, *64*, 3624.
(19) (a) Brouard, M.; Macpherson, M. T.; Pilling, M. J.; Tulloch, J. M.; Williamson, A. P. *Chem. Phys. Lett.* **1985**, *113*, 413. (b) Brouard, M.; Pilling, M. J. *Chem. Phys. Lett.* **1986**, *129*, 439.

0002-7863/87/1509-2916$01.50/0

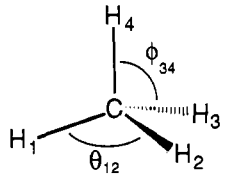

Figure 1. θ and ϕ angles for the H + CH_3 → CH_4 reaction. C–H4 is the bond being ruptured.

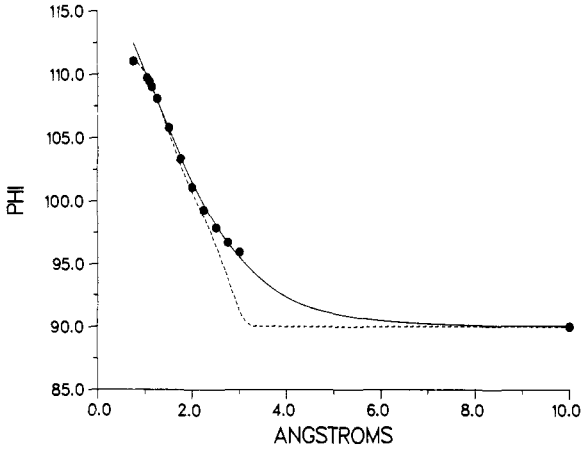

Figure 2. Optimized value for ϕ vs. R, $\phi_o(R)$. Solid circles give the ab initio result of Hirst, ref 13. The solid line is the fit by eq 1. The dashed line is the function of Duchovic et al., ref 11b. Angle is in degrees.

of Hirst,[13] as described below. The angular coordinates for the CH_4 system are defined in Figure 1, where the rupturing bond C–H4 is symbolized by C–H*, the H–C–H* angles are denoted by ϕ, and the H–C–H angles are denoted by θ. Along the H + CH_3 → CH_4 reaction path the optimized H–C–H* angle ϕ_o changes from 90° to the tetrahedral value 109.47°. Similarly, the optimized H–C–H angle θ_o changes from 120° to 109.47°.

The optimized values of ϕ_o and θ_o vs. C–H* bond length R, reported by Hirst, were fitted to the following equations:

$$\phi_o(R) = \phi_o^{CH_4} + (\phi_o^{CH_4} - 90.0)[S_\phi(R) - 1.0] \quad (1)$$

with $S_\phi(R)$ a switching function, given by

$$S_\phi(R) = 1.0 - \tanh\,[A_\phi(R - R_o)e^{B_\phi(R-C_\phi)^3}] \quad (2)$$

The parameters in eq 1 and 2 are $\phi_o^{CH_4} = 109.47°$, $A_\phi = 4.7418183 \times 10^{-1}$ Å^{-1}, $B_\phi = -2.6703827 \times 10^{-4}$ Å^{-3}, $C_\phi = 0.000$ Å, and $R_o = 1.086$ Å. The fit is found to be independent of C_ϕ values in the range of −1 to 1. $\theta_o(R)$ is given by

$$\theta_o(R) = \theta_o^{CH_4} + (\theta_o^{CH_4} - 120.0)[S_\theta(R) - 1.0] \quad (3)$$

$$S_\theta(R) = 1.0 - \tanh\,[A_\theta(R - R_o)e^{B_\theta(R-C_\theta)^3}] \quad (4)$$

where $\theta_o^{CH_4} = 109.47°$, $A_\theta = 7.7029473 \times 10^{-1}$ Å^{-1}, $B_\theta = -4.6616956 \times 10^{-3}$ Å^{-3}, and $C_\theta = 4.3805318$ Å. The above equations, (1)–(4), are eq 11–14 in ref 11b.

Since the parameters B_ϕ and B_θ are negative instead of positive, $S_\phi(R)$ and $S_\theta(R)$ do not have the correct limit of zero as $R \rightarrow \infty$. However, the two switching functions were chosen to accurately fit $\phi_o(R)$ and $\theta_o(R)$ for R as large as 10 Å, which is more than sufficient for this study.

The fit to Hirst's values for $\phi_o(R)$, eq 1, is given by the solid line in Figure 2. For comparison, the previous fit to eq 1 found by Duchovic et al.[11b] from MP4/6-31G** calculations is represented by the dashed line in Figure 2. For R less than approximately 2 Å the two curves are in good agreement. However, for larger R, the MRD–CI calculation of Hirst is seen to give a more gradual change in the optimized $\phi_o(R)$ values than that found from the MP4 calculations.

Hirst also calculated potential energies for displacements in the ϕ angles from their optimized values (Table III in ref 13). In these calculations, the θ angles were kept fixed at their optimized values. Results are reported for $R = 0.757$, 1.086, 1.5, 2.0, 2.5, 3.0, and 5.0 Å. Energies are given for a maximum ϕ displacement of 90°. To determine quadratic, cubic, and quartic ϕ force constants vs. C–H* bond length R, the energies at a particular R were fitted to the equation

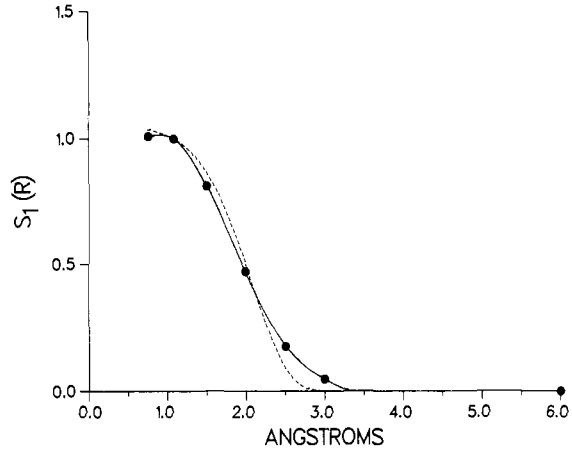

Figure 3. Switching function $S_1(R)$ for the quadratic ϕ force constant f_ϕ(R), eq 7. Solid circles give the ab initio result of Hirst, ref 13. The solid line is the fit by eq 7. The dashed line is the previous function of Duchovic et al., ref 11b.

$$V_\phi = \tfrac{1}{2}f_\phi(R)\sum_{i=1}^{3}[\phi_{i4} - \phi_o(R)]^2 + g_\phi(R)\sum_{i=1}^{3}[\phi_{i4} - \phi_o(R)]^3 + g_\phi(R)\sum_{i=1}^{3}[\phi_{i4} - \phi_o(R)]^4 \quad (5)$$

In order to obtain continuity in the cubic and quartic force constants vs. R, it was necessary to equate their values.

The resulting $f_\phi(R)$ and $g_\phi(R)$ force constants were fit to the equations

$$f_\phi(R) = S_1(R)f_\phi^{CH_4} \qquad g_\phi(R) = S_4(R)g_\phi^{CH_4} \quad (6)$$

where the switching functions $S_1(R)$ and $S_4(R)$ are given by

$$S_1(R) = 1.0 - \tanh\,[\alpha_1(R - R_o)(R - \beta_1)^{\gamma_1}]$$
$$S_4(R) = 1.0 - \tanh\,[\alpha_4(R - R_o)(R - \beta_4)^{\gamma_4}] \quad (7)$$

The terms $f_\phi^{CH_4}$ and $g_\phi^{CH_4}$ in eq 6 are the values for the force constants at the methane equilibrium geometry.

Duchovic et al.[11b] used the same switching function $S_1(R)$ for both $f_\phi(R)$ and $g_\phi(R)$. However, in order to accurately fit the more complete ab initio calculations of Hirst, different switching functions $S_1(R)$ and $S_4(R)$ are required for $f_\phi(R)$ and $g_\phi(R)$. It was also necessary to make the parameter γ variable in the switching functions. In the previous expression for $S_1(R)$ it was fixed at 8. The parameters for $S_1(R)$ and $S_4(R)$ are

$$\alpha_1 = 0.504\,537\,52 \qquad \alpha_4 = 0.383\,876\,89$$
$$\beta_1 = 0.419\,109\,20 \qquad \beta_4 = -0.169\,915\,27$$
$$\gamma_1 = 0.698\,926\,03 \qquad \gamma_4 = 0.971\,186\,70$$

Plots of $S_1(R)$ and $S_4(R)$ are given in Figures 3 and 4. The circles in these figures are values for the switching functions derived from Hirst's MRD–CI ab initio calculations. The solid lines are the fits to these points described above. The dashed line in each figure is the previous $S_1(R)$ function derived by Duchovic et al. from their MP4 calculations. For R less than approximately 2 Å, the MRD–CI and MP4 $S_1(R)$ curves are in good agreement. However, the attenuation of the MRD–CI switching function is more gradual for larger R. Comparing the curves in Figures 3 and 4 shows that the $S_1(R)$ and $S_4(R)$ switching functions are very similar.

Hirst's ab initio calculations yield values of 0.6758 mdyn·Å/rad^2 and −0.1134 mdyn·Å/rad^3 (ref 4) for the quadratic and cubic (quartic) ϕ force constants at the methane equilibrium geometry. In the previous work of Duchovic et al.[11b] it was found that a value

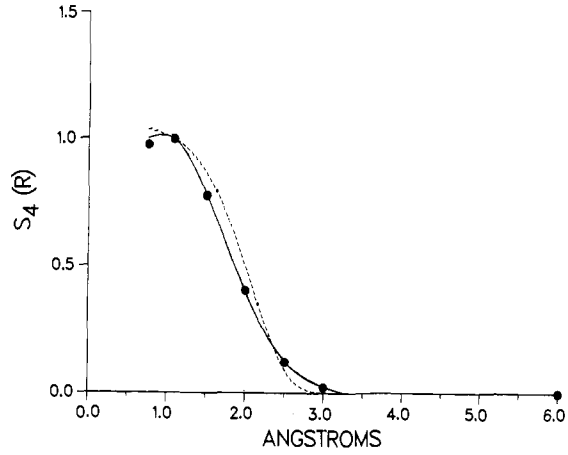

Figure 4. Same as Figure 3, but for the cubic/quartic ϕ force constant switching function $S_4(R)$.

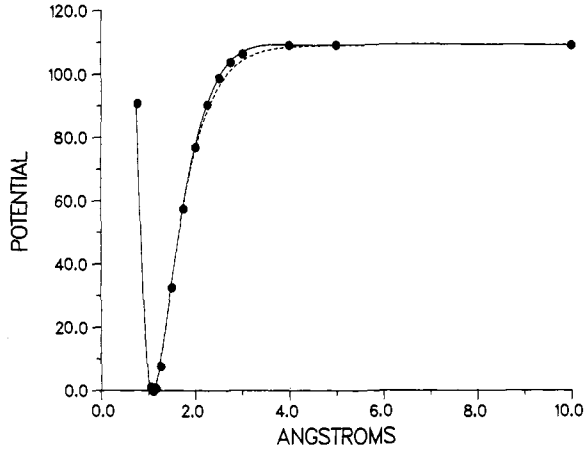

Figure 5. The Hirst ab initio CH stretching potential, ref 13, is given by the solid circles. The solid line is the fit to these points with the generalized Morse function. The dashed line is the normal Morse function. Potential is in kcal/mol.

of 0.5938 mdyn·Å/rad^2 for the quadratic ϕ force constant is required to reproduce the methane harmonic HCH bending frequencies. This value is maintained in the current surface for $f_\phi^{CH_4}$. Thus, in order not to alter the shape of the ϕ bending potential energy surface determined by Hirst, it is necessary to scale the cubic/quartic force constant so that $g_\phi^{CH_4}$ is equal to $-0.1134 \times (0.5938/0.6758) = -0.09964$.

The MRD–CI ab initio C–H stretching potential $V(R)$ calculated by Hirst is shown by the filled circles in Figure 5. In the calculations, the CH_3 geometry is optimized at each C–H* bond length R. The well depth D_e of 109.46 kcal/mol, the C–H* stretching harmonic force constant of 5.748 mdyn/Å, and the equilibrium bond length R_e of 1.0896 Å are in excellent agreement with the respective MP4 values of 110.6 kcal/mol, 5.739 mdyn/Å, and 1.086 Å.[11a]

A generalized Morse function, with β expressed by the cubic polynomial

$$\beta = A(R - R_e)^3 + B(R - R_e)^2 + C(R - R_e) + \beta_0 \quad (8)$$

is used to represent the MRD–CI CH stretching potential: where $A = 0.04194854$ Å^{-4}, $B = 0.03664173$ Å^{-3}, $C = -0.008502806$ Å^{-2}, $\beta_0 = 1.942142$ Å^{-1}, and $R_e = 1.0896$ Å. This function is given by the solid line in Figure 5. The dashed line is the standard Morse curve. It is seen that the ab initio potential energy rises more steeply and bends more sharply than the standard Morse potential. Because of the ab initio curve's shape, it is called a "stiff" Morse potential.[16a]

The combined $V(\phi)$ and $V(R)$ potential energy surface derived from Hirst's ab initio data is displayed in Figure 6. The angle χ is used to define a symmetric displacement of the ϕ angles in

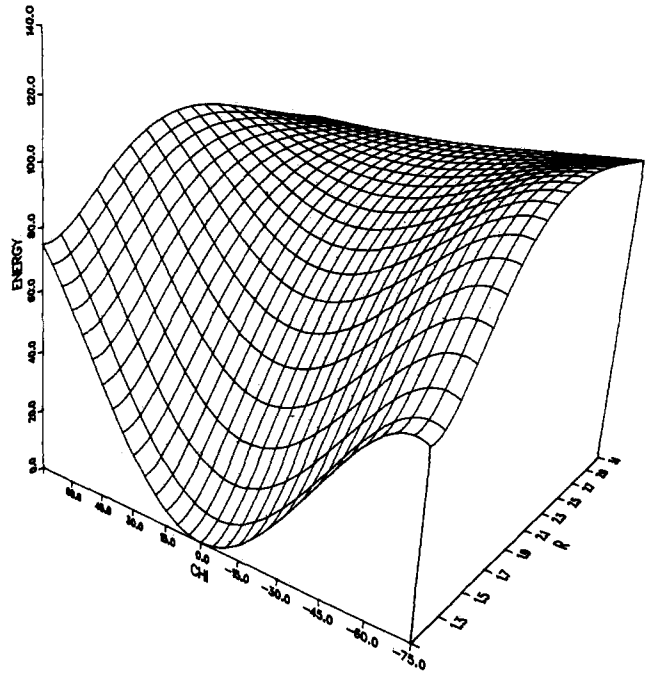

Figure 6. The H + $CH_3 \rightarrow CH_4$ potential energy surface. χ defines a symmetric displacement of the ϕ angles with $\phi_{42} = \phi_{43}$ (Figure 1). Positive χ denotes a decrease in ϕ_{41} and negative χ an increase. Potential energy is in kcal/mol.

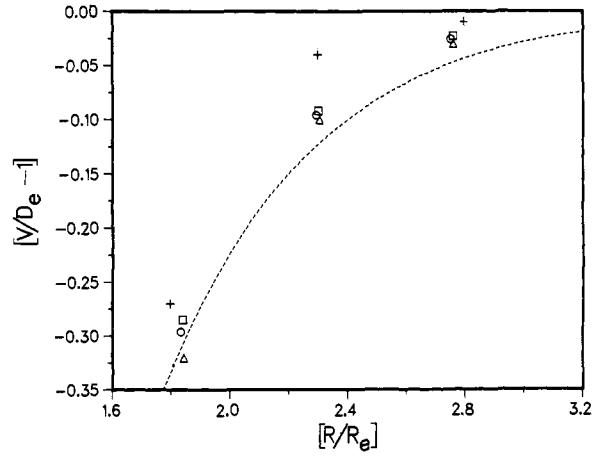

Figure 7. Plot of generalized parameters $[V(R)/D_e - 1]$ vs. R/R_e for the CH stretching potential: +, □, ○, and △ are the ab initio results of Duchovic et al. (ref 11a), Schlegel (ref 14), Hirst (ref 13), and Brown and Truhlar (ref 12), respectively. The dashed line is the Morse curve given by Hirst's results.

which $\phi_{42} = \phi_{43}$ (Figure 1). Positive χ denotes a decrease in ϕ_{41} and negative χ an increase in ϕ_{41}.

In Figure 7, comparisons are made between different ab initio calculations of the CH stretching potential. The points are presented in terms of the reduced potential, where $[V(R)/D_e - 1]$ is plotted vs. R/R_e. Included are the MP4/6-31G** calculations of Duchovic et al., the MRD–CI/6-31G** calculations of Hirst,[13] the MRD–CI calculations of Brown and Truhlar in which the 6-31G** basis is supplemented with C and H diffuse functions and an f-type subshell on C,[12] and the spin-projected MP4/6-31G** calculations of Schlegel.[14] The dashed line is the Morse reduced potential curve found from Hirst's ab initio values of β_e, R_e, and D_e.

Canonical variational transition state theory rate constants are calculated with the ab initio CH stretch potential energy curves determined by Hirst, Brown and Truhlar, and Schlegel. As will be shown in section IV, the canonical variational transition state theory rate constants are very sensitive to the shape of the CH stretching potential for R greater than 2.00 Å. Thus, it is necessary

to obtain very accurate fits to the ab initio potential points at these bond lengths. (The fit given above for the complete Hirst $V(R)$ curve is not sufficiently accurate at $R > 2.00$ Å for the canonical variational transition state theory calculations.) The accuracy of the fit was improved by making the Morse parameters D_e and R_e variables in addition to the variables A, B, C, and β_0 in eq 8. Only potential energy points for $R \geq 1.50$ Å were included in these fits. The resulting generalized Morse function parameters for the Hirst potential are $D_e = 103.4320$ kcal/mol, $R_e = 1.001500$ Å, $A = -1.017234 \times 10^{-3}$ Å^{-4}, $B = 7.7738886 \times 10^{-2}$ Å^{-3}, $C = 7.703640 \times 10^{-2}$ Å^{-2}, and $\beta_0 = 1.686690$ Å^{-1}; those for the Brown–Truhlar potential are $D_e = 98.6742$ kcal/mol, $R_e = 1.169340$ Å, $A = -1.553942 \times 10^{-5}$ Å^{-4}, B = 2.848116×10^{-2} Å^{-3}, C = 1.730306×10^{-1} Å^{-2}, and $\beta_0 = 1.880326$ Å^{-1}; and those for the Schlegel potential are $D_e = 122.4224$ kcal/mol, $R_e = 0.951859$ Å, $A = 0$, $B = 6.214863 \times 10^{-2}$ Å^{-3}, $C = 1.344940 \times 10^{-1}$ Å^{-2}, and $\beta_0 = 1.680627$ Å^{-1}.

To conclude this section, the potential energy surface used in the H + CH_3 → CH_4 canonical variational transition state theory calculations is reviewed. Except for the new switching function $S_4(R)$, eq 7, and the introduction of the parameters γ_1 and γ_4 into $S_1(R)$ and $S_4(R)$, the analytic potential energy function is the same as that derived by Duchovic et al.[11b] Hirst's ab initio calculations[14] are used to refit $\phi_0(R)$, $f_\phi(R)$, and $g_\phi(R)$. The ab initio C–H stretching potentials of Hirst,[13] Brown and Truhlar,[12] and Schlegel[14] are used in the canonical variational transition state theory calculations. These potentials are accurately fitted for values of $R \geq 1.5$ Å.

III. Reaction Path and Variational Calculations

The reaction path $r^\ddagger$ and properties associated with it were evaluated as described in part II,[16b] and only a brief outline is given here.[20] The reaction path is given by the steepest descent path, in mass-weighted Cartesian coordinates, from reactants, H + CH_3, to product, CH_4. The differential equations for determining the reaction path were numerically integrated with a fourth-order Runge–Kutta algorithm with a fixed step size of 0.000125 amu$^{1/2}$·Å. This calculation gives the geometry and classical potential energy $V_{MEP}(r^\ddagger)$ along the reaction path. The three principal moments of inertia $I_i(r^\ddagger)$ are calculated from the geometry.

Generalized normal coordinates and associated harmonic frequencies may be calculated for the motions orthogonal to the reaction path.[20] These properties are found by diagonalizing the projected force constant matrix $\mathbf{F}^P$ at points along the reaction path. $\mathbf{F}^P$ is found by projecting out of $\mathbf{F}$, a $3N \times 3N$ matrix of the mass-weighted Cartesian force constants, the direction along the reaction path, and the directions corresponding to infinitesimal rotations and translations. As a result of the projection, $\mathbf{F}^P$ will have seven zero eigenvalues corresponding to infinitesimal rotations, translations, and motion along the reaction coordinate. There will also be $3N - 7$ nonzero eigenvalues which give the harmonic frequencies $\nu_i(r^\ddagger)$ for the vibrations orthogonal to the reaction path.

The vibrational motions which undergo the most significant frequency changes along the reaction coordinate are (1) the bending motion which changes from an out-of-plane bend in CH_3 to a deformation in CH_4 and (2) the degenerate transitional rocking motions which change from rotations in H + CH_3 to deformations in CH_4. A plot of the natural logarithm of the transitional rocking frequency vs. C–H* bond length R is given in Figure 8. The frequency is for the surface which includes the fit to Hirst's complete $V(R)$ curve. The surfaces which incorporate fits to the Brown–Truhlar and Schlegel $V(R)$ curves give nearly identical results, since the frequency primarily depends on the switching function $S_1(R)$, eq 7.

In the statistical adiabatic channel model of Troe[8] it is assumed that the frequencies for the transitional rocking modes decrease

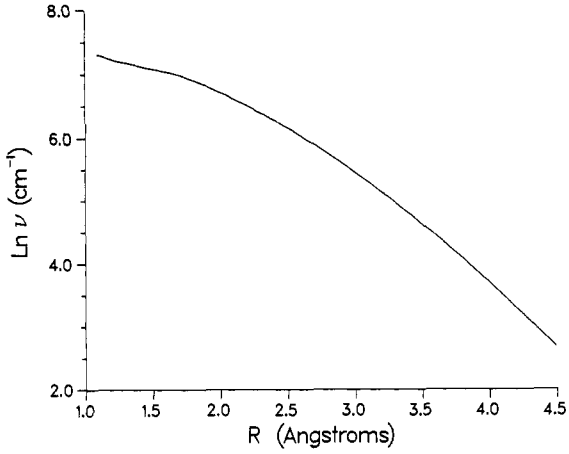

Figure 8. Natural logarithm of the harmonic frequency for the H---CH_3 transitional rocking mode vs. CH bond length.

exponentially as R is increased. The plot in Figure 8 shows that this is a good approximation for the H + CH_3 ⇄ CH_4 system over a limited range of R. For example, with R equal to 3.00–4.00 Å the slope of the curve in Figure 8 is −1.77 Å^{-1} with a correlation coefficient of −1.00. As will be discussed in the next section, transition states for $T = 200$–1000 K have values of R which range from 3.00 to 3.50 Å. For this R range the slope is −1.65 Å^{-1}, which is similar to the values −1.55 and −1.41 Å^{-1} found for the nondegenerate transitional rocking modes in H + HCO ⇄ H_2CO.[8c] Cobos and Troe[8b] have found, in fitting the statistical adiabatic channel model to a large number of experimental association rate constants, that the above slope divided by the Morse β parameter is equal to 0.46 (±0.09). A comparable value may be computed for H + CH_3 ⇄ CH_4 for R in the 3.00–3.50-Å range. At 3.25 Å β is 2.51 Å^{-1} for the surface which includes the fit to Hirst's complete $V(R)$ curve. The slope/β ratio is 1.65/2.51 = 0.66, and it is in fair agreement with the empirical estimate of Troe. It should be noted that this estimate assumes the stretching potential is given by a standard Morse function. Stiffening the stretching potential, as found with the ab initio calculations, will increase the slope/β ratio required in the statistical adiabatic channel model.[8d] This will improve the agreement between the present and estimated ratio.

The harmonic vibrationally–rotationally adiabatic ground-state potential $V_a^G(r^\ddagger)$ may be calculated from the above reaction path properties:

$$V_a^G(r^\ddagger) = V_{MEP}(r^\ddagger) + \sum_{i=1}^{3N-7} h\nu_i(r^\ddagger)/2 \qquad (9)$$

The canonical transition state is determined by finding the maximum of the standard-state generalized free energy of activation profile $G(r^\ddagger)$. To calculate $G(r^\ddagger)$, contributions to the free energy from the $3N - 7$ degrees of freedom orthogonal to the reaction path (including internal rotation) are summed and added to the free energy of external rotation and the vibrationally adiabatic potential:

$$G(r^\ddagger) = G_{vib}(r^\ddagger) + G_{ir}(r^\ddagger) + G_{rot}(r^\ddagger) + V_a^G(r^\ddagger) \qquad (10)$$

For all the calculations reported here, the internal degrees of freedom were treated as harmonic oscillators except for the low-frequency degenerate H---CH_3 transitional rocking motion. Comparison is made between the results of calculations in which these latter motions are treated as either a two-dimensional hindered internal rotor or as degenerate harmonic oscillators. The partition function for the two-dimensional hindered internal rotor is calculated classically according to

$$Q_{ir} = \frac{1}{\sigma h^2} \int e^{-H/kT} \, d\tau \qquad (11)$$

where the classical Hamiltonian is given by

$$H = p_\theta^2/2I + p_\phi^2/2I \sin^2\theta + V(\theta,\phi) \qquad (12)$$

(20) Details describing the determination of the reaction path and its associated properties may be found in the following: Miller, W. H.; Handy, N. C.; Adams, J. E. *J. Chem. Phys.* **1980**, *72*, 99.

Table I. H + CH_3 → CH_4 Transition State Parameters and Rate Constants for the Hirst Potential Surface

	vibrator[b]			hindered rotor[b]	
temp[a]	$R^{\ddagger}$	$\nu^{\ddagger}_{rock}$	k	$R^{\ddagger}$	k
200	3.54	95	1.24	3.67	1.37
300	3.42	118	1.43	3.55	1.59
400	3.33	138	1.56	3.45	1.73
500	3.25	157	1.64	3.37	1.84
600	3.19	173	1.70	3.29	1.92
800	3.09	204	1.78	3.17	2.05
1000	3.00	233	1.83	3.07	2.12

[a] Temperature is in K. [b] $R^{\ddagger}$ (Å) is the H---C distance at the transition state, $\nu^{\ddagger}_{rock}$ (cm^{-1}) is the vibrational frequency for the transitional rocking mode at the transition state, and k (10^{11} L mol^{-1} s^{-1}) is the rate constant.

The volume element $d\tau$ equals $dp_\phi d\theta d\phi dp_\theta$, where θ has the limits 0, π and ϕ has the limits 0, 2π. The symmetry number σ equals two for this CH_3 internal rotation. If $V(\theta,\phi)$ is zero, the partition function is that for free rotation and is $Q_{ir} = 8\pi^2 IkT/\sigma h^2$. The reduced moment of inertia I for the internal rotation was calculated as described by Pitzer and Gwinn,[21] i.e.

$$I = I_{CH_3}(1 - I_{CH_3}/I_{H\cdots CH_3}) \tag{13}$$

I_{CH_3} is the CH_3 moment of inertia and $I_{H\cdots CH_3}$ is the moment of inertia for the H---CH_3 system. The geometries for CH_3 and H---CH_3 are given by the Cartesian coordinates $r^{\ddagger}$ along the reaction path.

The reaction path and variational calculations reported here were performed with a modification of the general classical trajectory computer program MERCURY.[22] Standard expressions were used to relate the free energy terms in eq 10 to the partition functions.[23]

IV. Variational Transition State Theory Rate Constants

A. Hirst Potential Energy Surface. The H + CH_3 bimolecular rate constant vs. temperature was determined with canonical variational transition state theory, for the potential energy surface described in section II in which the Hirst ab initio $V(R)$ curve evaluated for $R \geq 1.50$ Å is fitted. Calculations were performed for both harmonic oscillator and hindered rotor treatments of the transitional rocking modes. The results are listed in Table I.

There is excellent agreement between the rate constants calculated by the two treatments of the transitional rocking modes. The rate constants slightly increase with increase in temperature. Also, a "tightening" of the transition-state structure is found with an increase in temperature, an effect that has been seen in other studies.[5]

B. Surfaces with the Brown–Truhlar and Schlegel $V(R)$ Curves. To compare with the above results for the Hirst surface, canonical variational transition state theory calculations were performed for surfaces in which the Brown–Truhlar and Schlegel ab initio $V(R)$ curves replace that calculated by Hirst. Only the harmonic oscillator treatment of the transitional rocking modes was considered in these calculations. The results are given in Table II.

A comparison of the rate constants in Tables I and II shows that those for the Hirst surface are intermediate between those for the Brown–Truhlar and Schlegel surfaces. Such a result was expected since the Hirst $V(R)$ curve is intermediate of the other two (Figure 7). However, the three sets of rate constants are in good overall agreement. As expected, the Brown–Truhlar surface, which has the most attractive $V(R)$ curve, gives rise to the "loosest" transition states. Also, the rate constants for the Brown–Truhlar surface show the least temperature dependence.

C. D + CH_3 → CH_3D Calculations. The results of the canonical variational transition state theory calculations for D + CH_3 are summarized in Table III. The transitional rocking modes were treated as classical hindered rotors in these calculations. Comparing the results in Tables I and III shows that $R^{\ddagger}$ is nearly the same for H + CH_3 and D + CH_3 association. The rate constants for H association are $2^{1/2}$ larger than those for D association.

Table II. H + CH_3 → CH_4 Transition State Parameters and Rate Constants for Surfaces with the Brown–Truhlar and Schlegel $V(R)$ Curves

	Brown–Truhlar surface[b]		Schlegel surface[b]	
temp[a]	$R^{\ddagger}$	k	$R^{\ddagger}$	k
200	3.55	1.50	3.50	1.03
300	3.43	1.65	3.39	1.20
400	3.33	1.74	3.29	1.32
500	3.26	1.80	3.22	1.40
600	3.19	1.84	3.16	1.47
800	3.09	1.89	3.06	1.56
1000	3.00	1.92	2.98	1.62

[a] Temperature is in K. [b] $R^{\ddagger}$ is the H---C distance at the transition state, and k (10^{11} L mol^{-1} s^{-1}) is the rate constant. The transitional rocking modes are treated as harmonic oscillators.

Table III. D + CH_3 → CH_3D Transition State Parameters and Rate Constants for the Hirst Potential Surface[a]

temp[b]	$R^{\ddagger}$	$\nu^{\ddagger}_{rock}$	k
200	3.66	72	0.99
300	3.54	90	1.14
400	3.44	107	1.24
500	3.35	124	1.32
600	3.27	140	1.37
800	3.16	170	1.48
1000	3.06	198	1.50

[a] The transitional rocking modes are treated as a 2-dimensional hindered rotor. The units and definitions for $R^{\ddagger}$, $\nu^{\ddagger}_{rock}$, and k are given in Table I. [b] Temperature is in K.

The isotope effect found in this work is what is predicted by transition-state theory for recombination reactions with loose transition states.[19b] The ratio of rate constants for H vs. D combination is

$$\frac{k_H}{k_D} = \left(\frac{m_D}{m_H}\right)^{3/2} \frac{Q^{\ddagger}_{rot,H}}{Q^{\ddagger}_{rot,D}} \frac{Q^{\ddagger}_{vib,H}}{Q^{\ddagger}_{vib,D}} \tag{14}$$

where equal total masses for the H---CH_3 and D---CH_3 transition states are assumed. It is immediately evident that in the ratio of vibrational partition functions all terms cancel except those for the transitional rocking modes. Also, the ratio of rotational partition functions is well approximated by $\mu_{H,CH_3}(R^{\ddagger}_H)^2/\mu_{D,CH_3}(R^{\ddagger}_D)^2 \simeq m_H/m_D$. Thus

$$\frac{k_H}{k_D} \simeq \left(\frac{m_D}{m_H}\right)^{1/2} \frac{Q^{\ddagger}_{tm,H}}{Q^{\ddagger}_{tm,D}} \tag{15}$$

where $Q^{\ddagger}_{tm}$ is the partition function for the two transitional rocking modes.

For a loose transition state with a large $R^{\ddagger}$ the ratio of the transitional rocking mode partition functions for H vs. D recombination is unity. The potential energy term is the same for both the H and D transitional rocking modes. In the hindered rotor treatment, eq 13 shows that the reduced moment of inertia equals I_{CH_3} for large $R^{\ddagger}$. Thus, the hindered rotor Hamiltonian, eq 12, is independent of D for H isotopic substitution. Likewise, in the harmonic oscillator treatment, the G element for a H—C---H(D) bend is independent of the H(D) mass at large $R^{\ddagger}$,[24] and the vibrational frequencies for the H---CH_3 and D---CH_3 rocking modes will be the same. Thus, for loose transition states, the isotope effect for H vs. D recombination is $(m_D/m_H)^{1/2}$.

(21) Pitzer, K. S.; Gwinn, W. D. *J. Chem. Phys.* **1942**, *10*, 428.
(22) Hase, W. L. *QCPE* **1980**, *11*, 453.
(23) Davidson, N. *Statistical Mechanics*; McGraw-Hill: New York, 1962; p 123.
(24) Wilson, E. B., Jr.; Decius, J. C.; Cross, P. C. *Molecular Vibrations*; McGraw-Hill: New York, 1955; pp 303–308.

Table IV. Comparison of Transitional Rocking Mode Partition Functions

		partition functions[a]		
T (K)	$R^{\ddagger}$ (Å)[b]	Q_{ir}	$Q_{ho,c}$	$Q_{ho,q}$
200	3.67	3.325	3.422	3.340
300	3.55	4.878	4.928	4.845
400	3.45	6.296	6.218	6.136
500	3.37	7.548	7.267	7.184
600	3.29	8.721	8.226	8.141
800	3.17	10.723	9.755	9.670
1000	3.07	12.578	11.184	11.102

[a] Q_{ir} is the classical hindered internal rotation partition function, $Q_{ho,c}$ is the classical harmonic oscillator partition function, and $Q_{ho,q}$ is the quantum harmonic oscillator partition function. [b] $R^{\ddagger}$ is the C---H bond length at the transition state determined by the classical hindered internal rotation treatment.

The transition states found in this work are sufficiently near the loose limit that the recombination isotope effect is $(m_D/m_H)^{1/2}$. At a particular $R^{\ddagger}$, the reduced moment of inertia for hindered internal rotation is nearly the same for H and D recombination. Likewise, as shown in Tables I and III, the H---CH_3 and D---CH_3 rocking frequencies are nearly identical at a particular $R^{\ddagger}$.

V. Discussion

One of the most significant results of this study is that the Hirst ab initio potential energy surface,[13] when combined with canonical variational transition state theory, gives H + CH_3 → CH_4 and D + CH_3 → CH_3D bimolecular rate constants which agree with the experimental values of Pilling and co-workers.[19] No adjustments are made in the ab initio potential energy surface parameters to attain this agreement. The experimental rate constant[19] is 2.8×10^{11} L mol^{-1} s^{-1} for H + CH_3 with T = 300–600 K, and 1.1×10^{11} L mol^{-1} s^{-1} for D + CH_3 with T = 290–400 K. For example, by treating the transitional rocking modes as hindered rotors, the calculated rate constants for these temperature ranges are $1.6–1.9 \times 10^{11}$ L mol^{-1} s^{-1} for H + CH_3 and $1.1–1.2 \times 10^{11}$ L mol^{-1} s^{-1} for D + CH_3 (Tables I and III). The effect of replacing the Hirst[13] CH stretching potential with those determined by Brown and Truhlar[12] and Schlegel[14] is a variation of less than 30% in the calculated rate constant. Rate constants calculated by treating the transitional rocking modes as either harmonic oscillators or classical hindered rotors differ by only 10–15% over the 200–1000 K temperature range. Clearly, much better agreement is found between theory and experiment in this work than was found previously.[16]

Though there is good overall agreement between the experimental and theoretical rate constants, it should be noted that the experimental and theoretical isotope effects are not in agreement. The ratio of the H + CH_3 and D + CH_3 association rate constants is 2.5 and 1.4 from the experimental and theoretical work, respectively. As discussed in the previous section, it is unlikely that transition-state theory can give an isotope effect as large as 2.5. Such an isotope effect would arise from dynamical attributes in the association reaction such as incomplete intramolecular vibrational energy redistribution within the molecule formed by association[25] and/or recrossing of the dividing surface separating reactants and products.[26]

In Table IV transitional rocking mode partition functions calculated by classical hindered internal rotor, classical harmonic oscillator, and quantum harmonic oscillator treatments are compared. The partition functions are calculated at different temperatures and for values of $R^{\ddagger}$ which define the internal rotor transition states. The difference between the classical internal rotor and harmonic oscillator partition functions is as large as 12%. However, the classical and quantal harmonic oscillator partition functions agree within 2% at all temperatures. As discussed in the following, excellent agreement is also expected between the classical and quantal hindered internal rotor partition functions.

In previous work, Pacey and co-workers[9,27] have calculated exact quantum partition functions for hindered internal rotation and compared them with those calculated with the quantal harmonic oscillator and classical hindered rotor approximations. They found for sinusoidal rotor potentials that, if the zero-point energy for the hindered rotor is less than or equal to $1.4k_bT$, the classical hindred rotor partition function agrees with the exact quantum partition function to within 10%.[27,28] This criterion is certainly met for the transition states considered here, and we expect that the partition function for the H + CH_3 → CH_4 transitional rocking modes is accurately determined by the classical hindered rotor treatment.

Partition functions for all internal degrees of freedom, except the transitional rocking modes, were calculated with the harmonic oscillator approximation. Though the vibrations have anharmonic character, the vibrational frequencies are nearly the same for the reactants and the transition state, and errors in the partition functions cancel in calculating the rate constant. The largest frequency shift (i.e., 50–140 cm^{-1} higher for the transition states at 200 and 1000 K, (respectively) is for the CH_3 out-of-plane vibration.

The variational transition state theory rate constant for H + CH_3 recombination and its temperature dependence are sensitive to details of the potential energy surface. A positive temperature dependence in the rate constant, which decreases as the H–CH_3 stretching potential becomes more attractive, has been found. In the work presented here, the Brown–Truhlar surface is the most attractive and shows the least temperature dependence. In previous calculations with the standard and stiff Morse potentials,[9] the rate constants found from the standard Morse potential show the least temperature dependence (the stiff Morse potential is based on MP4 ab initio results). Only the rate constant for the stiff Morse potential surface shows the $T^{1/2}$ dependence of the hard sphere collision model. The temperature dependence is much less for the surfaces investigated in the work presented here. For a sufficiently attractive potential, a negative temperature dependence in the H + CH_3 rate constant is expected. Potential energy surfaces derived for CH_3 + CH_3 and Li^+ + H_2O recombination give rate constants with a negative temperature dependence.[2a,29,30] In future work it would be interesting to investigate how changes in the attenuation of the potential for the transitional modes affects the temperature dependence of the rate constant.

The microcanonical variational method, in which transition states are determined as a function of angular momentum J and energy E, gives a lower bound to the thermal rate constant than the canonical method, in which only one transition state is found for each temperature.[4] To determine a thermal rate constant from the microcanonical transition states, the microcanonical rate constants $k(E,J)$ must be averaged by a numerical integration over Boltzmann E and J distributions. As a result, several orders of magnitude more computer time is required for the microcanonical calculation. Large differences have been found between canonical and microcanonical association rate constants for surfaces with highly attractive potentials, which have transition-state structures which are strongly energy (temperature) dependent. For example, in Li^+ + $(CH_3)_2O$ association,[31] the canonical rate constant is 37% and 6% larger at 200 and 1000 K, respectively. In a study of O + OH recombination on a surface which has an overly attractive long-range potential, significant differences are found between the canonical and microcanonical rate constants.[6] However, the canonical and microcanonical approaches have been found to give similar thermal rate constants for association on potential energy surfaces like those investigated

(25) Bunker, D. L.; Hase, W. L. *J. Chem. Phys.* **1973**, *59*, 4621. Hase, W. L. In *Dynamics of Molecular Collisions Part B*; Miller, W. H., Ed.; Plenum: New York, 1976; p 121.
(26) Swamy, K. N.; Hase, W. L. *J. Am. Chem. Soc.* **1984**, *106*, 4071.
(27) LeBlanc, J. F.; Pacey, P. D., private communication.
(28) Also see: Frisch, M. J.; Liu, B.; Binkley, J. S.; Schaefer, H. F., III; Miller, W. H. *Chem. Phys. Lett.* **1985**, *114*, 1.
(29) Mondro, S. L.; Vande Linde, S.; Hase, W. L. *J. Chem. Phys.* **1986**, *84*, 3783.
(30) Wardlaw, D. M.; Marcus, R. A. *J. Phys. Chem.* **1986**, *90*, 5383.
(31) Vande Linde, S.; Mondro, S. L.; Hase, W. L. *J. Chem. Phys.* **1987**, *86*, 1348.

here. Two different studies of methyl radical recombination found the canonical rate constant to be 1.07 and 1.20 times larger.[2a,30] For C-H split in propylene the canonical and microcanonical rate constants agree to within 10%.[32] Nearly exact agreement is found between the two rate constants for surfaces with well-defined barriers and, thus, have transition states which are only weakly dependent on energy and/or temperature.[33] From these comparisons, the canonical variational transition state method is expected to be accurate for calculating the $H + CH_3 \rightarrow CH_4$ thermal rate constant.

Acknowledgment. This research was supported by the National Science Foundation. Professors H. B. Schlegel and P. D. Pacey are thanked for helpful discussions.

(32) Naroznik, M.; Niedzielski, J., private communication.

(33) Isaacson, A. D.; Sund, M.; Rai, S. N.; Truhlar, D. G. *J. Chem. Phys.* **1985**, *82*, 1338.

Theory and Experiment in Concert: Evidence for a Stable Ammoniaborene Dication (H_3NBH^{2+})†

Thomas Drewello,‡ Wolfram Koch,‡ Carlito B. Lebrilla,‡ Daniel Stahl,⊥ and Helmut Schwarz*‡

Contribution from the Institut für Organische Chemie der Technischen Universität Berlin, D-1000 Berlin 12, West Germany, and the Institut de Chimie Physique, Ecole Polytechnique Federale de Lausanne, CH-1015 Lausanne, Switzerland. *Received November 14, 1986*

Abstract: The potential energy surfaces of the mono- and dications of aminoborane (NH_2BH_2) and ammoniaborene (NH_3BH) were explored by high level ab initio calculations. Although two minima were located on either surface, corresponding to $NH_2BH_2^{+\bullet}$, $NH_3BH^{+\bullet}$, $NH_2BH_2^{2+}$, and NH_3BH^{2+}, the theoretical analysis, in conjunction with charge stripping mass spectrometry, suggests that the only dication formed is that of ammoniaborene (NH_3BH^{2+}), requiring a Q_{min} value of 15.2 eV. NH_3BH^{2+} is predicted to be 60.6 kcal/mol more stable than the $NH_2BH_2^{2+}$ which is due to the powerful donor/acceptor interactions operative in NH_3BH^{2+}. Comparison of the $BNH_4^{+\bullet}/BNH_4^{2+}$ ions with the isoelectronic $C_2H_4^{+\bullet}/C_2H_4^{2+}$ species is made.

There has been considerable interest in aminoborane as a candidate for an inorganic analogue of ethylene.[1] Microwave spectroscopy has provided ample evidence that the neutral produced from the pyrolysis of the ammonia/borane mixture is a planar H_2NBH_2 species **1** similar to ethylene.[2]

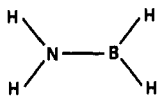

1

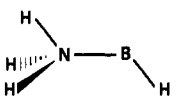

2

More recently,[3b] with the aid of He I photoelectron spectroscopy and a combination of semiempirical/ab initio calculations, a twisted form of $\mathbf{1}^{+\bullet}$ was assigned for $NH_2BH_2^{+\bullet}$. We have produced dicationic BNH_4^{2+} by applying charge stripping mass spectrometry[4] to mass-selected $BNH_4^{+\bullet}$ which in turn was produced by 70 eV electron impact ionization of aminoborane. The latter was generated as described in ref 2 and 3. Our experimental findings are complemented by ab initio MO calculations.[5] Optimized geometries, zero-point energies (ZPE), and harmonic frequencies were calculated with the 6-31G(d) basis set.[6] Minima and transition structures were characterized by having the correct number of negative eigenvalues of the Hessian matrix (no negative eigenvalue for the former and one for the latter). Single-point calculations were performed with the 6-311G(d,p) basis set.[7] Effects of valence electron correlation were incorporated by means of Møller-Plesset perturbation theory terminated at the 4th order.[8] All data reported in Figures 1 and 2 refer to this level of theory (MP4/6-311G(d,p)//6-31G(d) + ZPE). Ionization energies, IE, were calculated assuming vertical ionization. Geometries (bond

Table I. Total Energies (in hartrees) and ZPE (in kcal/mol) for Mono- and Dicationic BNH_4 Species, Transition Structures, and Some Dissociation Products

structure	6-31G(d)	MP4/6-311G(d,p)	ZPE[a]
H_3NBH^+	-81.15382	-81.45543	29.5
		-80.87455[b]	
$H_2NBH_2^+$	-81.15769	-81.44648	26.3
		-80.74519[b]	
$H_2NBH_2^+ \rightarrow H_3NBH^+$ TS	-81.07124	-81.39392	25.8
H_2NBH---H^+ TS	-81.10625	-81.42372	23.2
H_2NBH^+	-80.61302	-80.91016	21.9
H_3NBH^{2+}	-80.63102	-80.92196	29.1
$H_2NBH_2^{2+}$	-80.49264	-80.81418	25.1
$H_2NBH_2^{2+} \rightarrow H_3NBH^{2+}$ TS	-80.46794	-80.79739	23.8
H_2NBH---H^{2+} TS	-80.46794	-80.79740	23.8
H_2NBH^+	-80.61302	-80.91018	21.9
H_3N---BH^{2+} TS	-80.52462	-80.78613	26.2
BH^+	-24.81518[c]	-24.86374[c]	3.6
H_3N^+	-55.87324[c]	-56.06987[c]	19.8
H---H_2NBH^{2+} TS	-80.48262	-80.77911	22.8
H_3NB---H^{2+} TS	-80.44145	-80.74695	24.0
H_3NB^+	-80.52528	-80.83145	23.5
H_2N---BH_2^{2+} TS	-80.41604	-80.69504	23.5
BH_2^+	-25.47080[c]	-25.55277[c]	10.4
H_2N^+ ($^1A_1$)	-55.12729[c]	-55.30390	10.9

[a] Scaled by a factor of 0.9. See the following: Pople, J. A.; Schlegel, H. B.; Krishnan, R.; DeFrees, D. J.; Binkley, J. S.; Frisch, M. J.; Whiteside, R. A.; Hout, R. F.; Hehre, W. J. *Int. J. Quant. Chem., Symp.* **1981**, *15*, 269. [b] Dication from fixed monocation structure. [c] *The Carnegie-Mellon Quantum Chemistry Archive, Third Edition*; Whiteside, R. A., Frisch, M. J., Pople, J. A., Eds.

† Dedicated to Professor Hans-Werner Wanzlick, Berlin, on the occasion of his 70th birthday.

‡ Berlin.

⊥ Lausanne.

0002-7863/87/1509-2922$01.50/0